(Received 14 October 2024, Accepted 3 January 2025, Scheduled 18 January 2025)

A Broadband Half-Mode Substrate Integrated Waveguide Cavity Antenna with Triple Resonances

Dian Widi Astuti[1, *], Huda A. Majid[2], Syah Alam[3], and Andri Setyawan[1]

[1] *Universitas Mercu Buana, Jakarta 11650, Indonesia*
[2] *Universiti Tun Hussein Onn Malaysia, Johor 86400, Malaysia*
[3] *Universitas Trisakti, Jakarta 11450, Indonesia*

ABSTRACT: A simple, low-profile, compact, and broadband antenna is presented in this paper. The compact antenna is achieved through a 50% miniaturization of a full-mode substrate-integrated waveguide (FMSIW) antenna, known as half-mode substrate-integrated waveguide (HMSIW). The low-profile antenna is the result of the thin substrate thickness. However, the miniaturized and low-profile antenna suffers from narrow impedance bandwidth, which limits its application in antenna implementations. To address this issue, this paper proposes a broadband antenna in a single HMSIW cavity, offering a simple solution. The broadband performance is achieved by the merging of triple resonances. These triple resonances are generated by the combination of TE_{101}, TE_{102}, and TE_{202} modes, which are induced by a semi-rectangular ring slot on the top layer of the cavity. Good agreement is observed between the simulation and measurement results. The simulated fractional bandwidth (FBW) is 29.53% (9.67–13.02 GHz), while the measured FBW is 32.05% (9.51–13.14 GHz). Two identical antennas with different polarization directions are obtained by mirroring one of them to the other.

1. INTRODUCTION

Substrate-integrated waveguide (SIW) antenna, initially a waveguide transmission line, can be easily implemented through substrate development. It offers a high-quality antenna with the consequence of a narrow bandwidth [1] for a cavity-backed slot antenna (CBSA) type. A narrow bandwidth in the SIW CBSA can be solved by substrate removal [2], stacked substrate layers [3], slot modification [4–7], a shorting via [8, 9], metamaterial used [10, 11], dielectric resonator [12], slot array [13], and metasurface [14].

The suggested approach in [2] eliminates the substrate beneath the slot to lower its capacitance. Given that a half-wavelength slot acts as a parallel resonant circuit at its resonant frequency, reducing the capacitance enhances the antenna's bandwidth. The 10-dB fractional bandwidth (FBW) of the fabricated antenna, as measured, was 2.16% by using this method. The research idea involves replacing the conventional rectangular cavity slot with a modified bow-tie cavity slot proposed by [3]. The primary function of the cavity coupling slot is to optimize the energy transfer from the rectangular waveguide feed into the cavity layer, which is crucial for the overall performance of both the subarray and the array antenna system in stacked substrate layers. The fabricated fixed-beam 8×8 cavity-backed slot array antenna has achieved a broadband impedance bandwidth of 28% (23–31 GHz). However, the alignment of the stacked layer substrates has to be noticed.

The slot modification for bandwidth enhancement is proposed by [4–6]. Ref. [4] proposes a modified dumbbell-shaped slot antenna and a coplanar waveguide feeding structure on the ground for generating high-order resonant modes. The five resonances for bandwidth enhancement are achieved in the measured antenna with 26.7% (18.2–23.8 GHz) of FBW. The modified I-shaped slot with square and C shape slots is used in [5] for the bandwidth enhancement method by generating dual-resonances. The measured impedance bandwidth of 19.04% is achieved for the X-band frequency range. The combination of hexagonal and rectangular slots is used for expanding impedance bandwidth as reported by [6]. Dual-resonances are achieved with a 21.6% of FBW. The slot modification for the bandwidth enhancement looks like a simple method. However, the slot placement has to be addressed according to electric field spreading, and it is not an easy task.

By using shorting vias on the half bow-tie complementary-ring slot, [8] creates dual-resonances for expanding impedance bandwidth. By incorporating three shorting vias on either the left or right side of the half bow-tie complementary-ring slot, the resonances of the higher mode and lower mode are reduced to below -10 dB. A 14.81% of FBW is achieved in the measurement result. A shorting via on the T-shaped slot enhances impedance bandwidth, resulting in triple resonances as reported by [9], and the antenna measurement has a 5.76% FBW that covers the frequency range 6.75–7.15 GHz. A shorting via has been successfully implementation for bandwidth enhancement. However, shorting vias placement is not an easy task.

Implementation of a metamaterial unit cell such as a split ring resonator that is placed on the right and left of the feeding line has been proven for bandwidth enhancement as shown in [10]. As a result, the FBW of 13.2% is achieved for millimeter wave application. Therefore, employing a split ring resonator struc-

* Corresponding author: Dian Widi Astuti (dian.widiastuti@mercu-buana.ac.id).

ture with the SIW antenna results in a wideband that is three times greater than the conventional bandwidth of an SIW antenna. Negative index metamaterial has been implemented into the SIW Vivaldi antenna for bandwidth enhancement as shown in [14]. The negative index metamaterial has set up a 7×3 unit cells array. The metamaterial unit cells array is placed next to the antenna radiation. Metamaterial design can be used as an option for a method of enhancing bandwidth. However, the antenna measurement reflection coefficient has a frequency shift differentiation of 2.5 GHz [11].

Dielectric resonators can be used for bandwidth enhancement as shown in [12]. Dielectric resonators are constructed from low-loss materials with high permittivity, making them a promising option for microwave and millimeter wave communication systems. The cylindrical, hemispherical, and rectangular shape dielectric resonators have been proven for bandwidth enhancement methods. Antennas with different shape dielectric resonators have a wider impedance bandwidth (average 12.64% of FBW) than those without dielectric resonators used (1% of FBW). However, the addition of the dielectric resonator made the antenna dimension thick, especially on the radiation part.

Two parallel slots of unequal lengths are used in [13] for the bandwidth enhancement method. In general, long slots are used for transmitting while short slots are used for matching. To suppress the mutual coupling between adjacent array antennas, a non-resonant slot is etched in the separation arrays. A measured FBW of 9.42% is achieved by using this method at 24 GHz. However, the antenna dimension is larger than the single antenna.

A modified spiral slot resonator as unit cells of metasurface is used for bandwidth enhancement as shown in [14]. A metasurface antenna is positioned at the top, featuring tilted slots. This method succeeded in 7.62% of FBW even though the thickness of the antenna became bulky. All of the references above are used full-mode SIW (FMSIW).

Miniaturization can be done easily on the FMSIW antenna by dividing it symmetrically. Fraction modes such as half-mode SIW (HMSIW) [15–17], quarter-mode SIW (QMSIW) [18–20], eighth-mode SIW (EMSIW) [21–28], sixteenth-mode SIW (SMSIW) [29, 30], and sixty-fourth-mode SIW (SFMSIW) [31] result from miniaturization. The miniaturization of SIW antenna has been used widely for multiband antenna. However, the smaller the dimensions of the antenna are used, the more limited the transverse electric (TE) mode works on the antenna. Eventually, only the TE_{101} mode is dominant, and the antenna has a single resonance and suffers from a low FBW.

Furthermore, not all of the bandwidth enhancement methods on the FMSIW above [2, 3, 12–14, 4–11] can be implemented on the fraction mode SIW. Some methods such as modification slot [32–34], dual-cavities [35–37], defected ground structure [38], and mutual coupling [39–42] are used to get a higher FBW by resulting in multi-resonances. However, few references have the FBW of more than 30%.

This paper presents an HMSIW antenna with a high fractional bandwidth in a single cavity layer for X-band applications. The key contributions of this paper are as follows:

1. The broadband impedance bandwidth is achieved by merging multiple modes. This multi-resonance merging is excited using a simple slot, i.e., a half-rectangular ring slot shape. The proposed antenna achieves an impedance bandwidth simulation of 29.53% (9.67–13.02 GHz).
2. Two identical antennas with different polarization directions, namely RHCP (Right-Hand Circular Polarization) and LHCP (Left-Hand Circular Polarization), are obtained by mirroring one of them.
3. A good agreement between simulation and measurement results is achieved. The measured FBWs are 32.05% (9.51–13.14 GHz) for the RHCP and 30.39% (9.46–12.85 GHz) for the LHCP.
4. An easy analysis of TE mode merging because of using a single cavity.
5. A low profile ($0.04\lambda_g$ at 11.33 GHz) and a compact antenna by utilizing the HMSIW structure.

2. ANTENNA DESIGN

2.1. Antenna Evolution

The proposed antenna design is similar to the previous published research [36]. However, the proposed antenna design offers a simple slot and an easy analysis of TE mode in the single cavity. This design is implemented on a single-layer Rogers Duroid RO 5880 substrate, which has a thickness of 1.575 mm, a dielectric constant of 2.2, and a loss tangent of 0.0009. Metallic vias are arranged in a rectangular pattern near the cavity's sidewall to form the half-rectangular SIW cavity. The diameter of the vias (d) and the spacing between the via centers (p) are specified according to SIW guidelines ($d/p \geq 0.5$ and $\lambda_0/d \geq 10$) [43], for minimizing losses through the ideal electric conductor wall.

The antenna's evolution achieves the proposed antenna design, as shown in Figure 1. The proposed antenna design starts with the rectangular FMSIW cavity. The dimensions of the rectangular FMSIW cavity are determined by applying the frequency to the antenna design, which can be calculated using Equation (1) [44], and in this research 10 GHz is the frequency implementation for the FMSIW cavity. A rectangular slot is

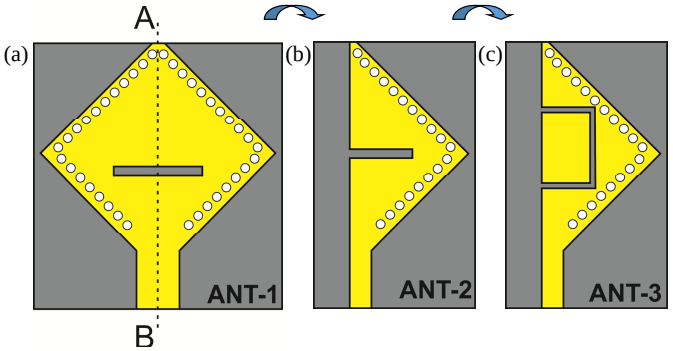

FIGURE 1. Antenna evolution: (a) FMSIW cavity with a rectangular slot antenna as a conventional SIW antenna, (b) HMSIW cavity used a half-rectangular slot, (c) HMSIW cavity used a half-rectangular ring slot antenna.

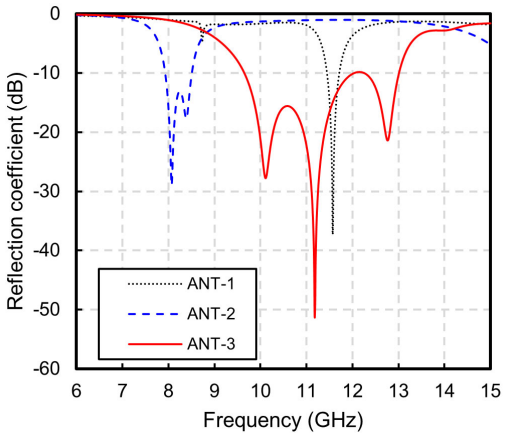

FIGURE 2. Reflection coefficient simulation for antenna evolution.

Parameter	Dimension (mm)	Description
Ws	18	The substrate width
Ls	30	The substrate length
d	1	The diameter hole
p	1.5	The distance between the two hole center
Wf	2.425	The feed width
Lf	6.5	The feed length
St	0.6	The slot thickness
Sl	20	The slot length
Sp	7	The slot gap
gap	4	Gap substrate

TABLE 1. Antenna parameters.

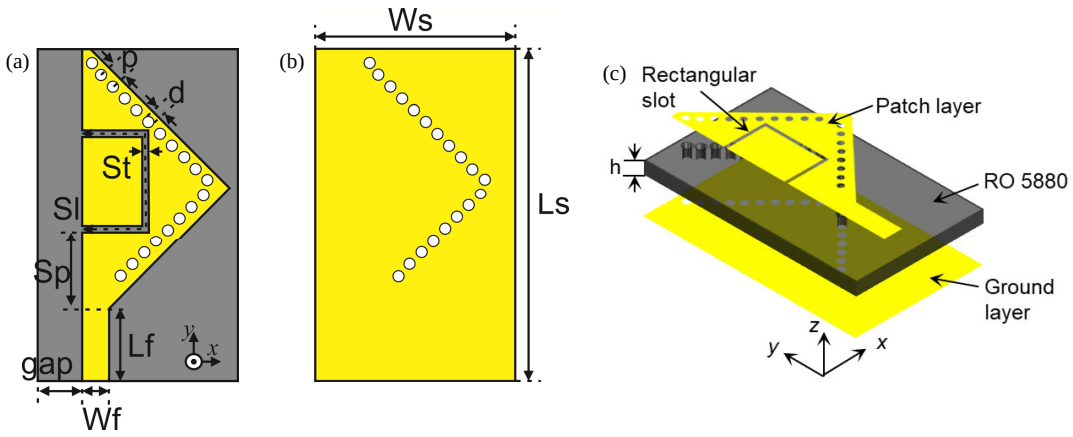

FIGURE 3. The geometric of the ANT-2 dimension: (a) the top layer, (b) the ground layer, (c) 3D antenna view.

added into the patch rectangular FMSIW cavity as a conventional SIW antenna displayed in Figure 1(a) (ANT-1).

$$f_{mnp}^{\text{SIW}} = \frac{c}{2\pi\sqrt{\mu_r\varepsilon_r}}\sqrt{\left(\frac{m\pi}{L_{eff}}\right)^2+\left(\frac{n\pi}{h}\right)^2+\left(\frac{p\pi}{W_{eff}}\right)^2} \quad (1)$$

The ANT-1 simulated reflection coefficient is below -10 dB across the frequency range of 11.45–11.71 GHz, which spans 260 MHz. ANT-1 has a single resonant frequency with 2.25% FBW as shown in Figure 2. ANT-1 suffers from a narrow impedance bandwidth and is divided vertically (AB) into two equal antenna sections for miniaturization dimension as named ANT-2 in Figure 1(b). The slot position of ANT-2 is shifted to the upper side for impedance bandwidth improvement and miniaturization.

ANT-2 has 0.58 GHz (7.93–8.51 GHz) impedance bandwidth with dual resonances on 8.07 GHz and 8.39 GHz and has a 7.06% FBW which means that FBW of ANT-2 enhances 3.14 times compared to ANT-1. The rectangular slot is extended to become one wavelength guided ($1.0\lambda_g$) on the frequency application chosen. Impedance bandwidth is enhanced significantly into 3.35 GHz that resonates at 9.67–13.02 GHz. 29.53% FBW is achieved on the ANT-3 design as shown in Figure 1(c). ANT-3 has triple resonances at 10.12, 11.18, and 12.77 GHz. All of the simulations of antenna design used the Ansys HFSS electromagnetic simulator.

Figures 3(a) and (b) show the geometrical two dimensions of the proposed antenna design for the top and ground layers while the exploded view of the proposed HMSIW antenna is shown in Figure 3(c). The final antenna dimensions are tabulated in Table 1.

2.2. Electric Field

The proposed antenna design has a broadband impedance bandwidth by generating triple resonances. The triple resonances consist of several adjacent TE modes joined together for broadband impedance bandwidth. The adjacent TE modes consist of TE_{101}, TE_{102}, and TE_{202} modes combination, and they can be analyzed by electric field spreading as shown in Figure 4–Figure 6.

Figure 4 shows the first resonance that occurs at 10.12 GHz. The electric field spreading on 10.12 GHz occurs because of the TE_{101} and TE_{102} modes blended. The clear electric field spreadings are shown by the phase step every 90°. The strong

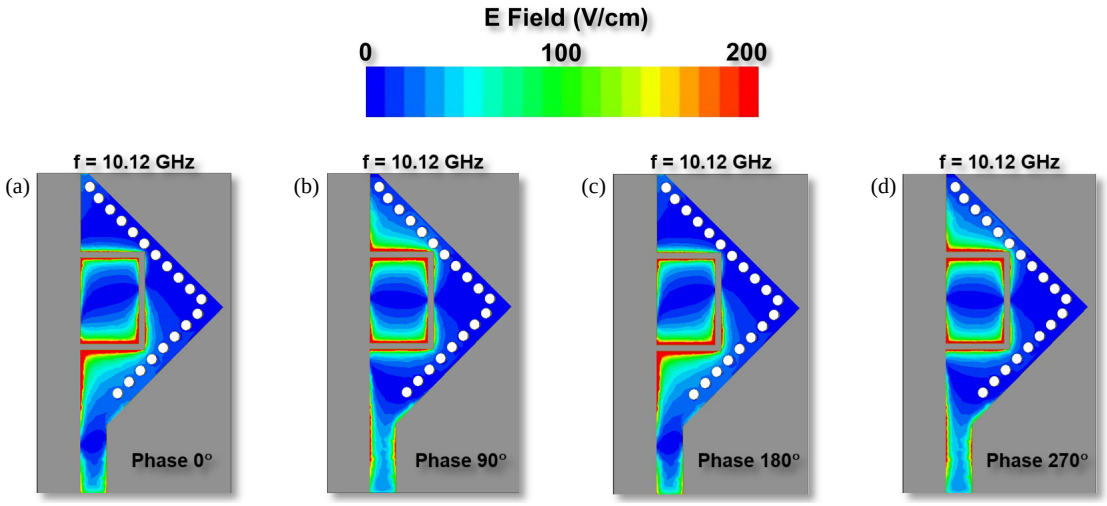

FIGURE 4. The electric field spreading on 10.12 GHz at phase: (a) 0°, (b) 90°, (c) 180°, and (d) 270°.

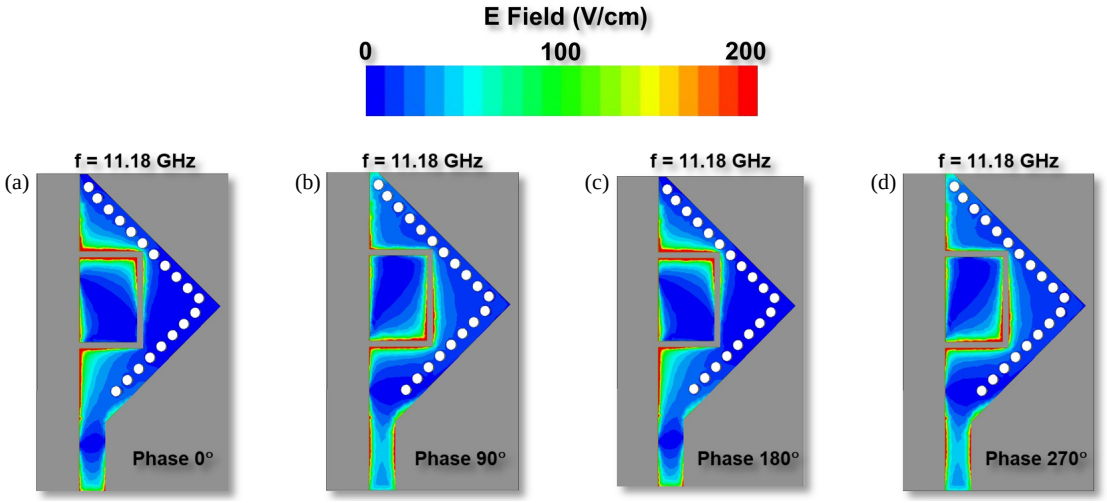

FIGURE 5. The electric field spreading on 11.18 GHz at phase: (a) 0°, (b) 90°, (c) 180°, and (d) 270°.

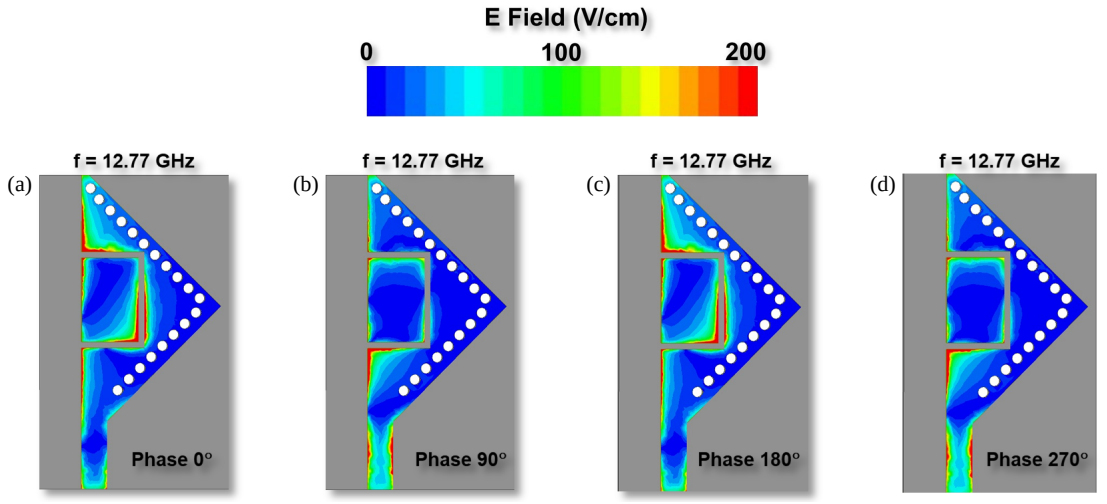

FIGURE 6. The electric field spreading on 12.77 GHz at phase: (a) 0°, (b) 90°, (c) 180°, and (d) 270°.

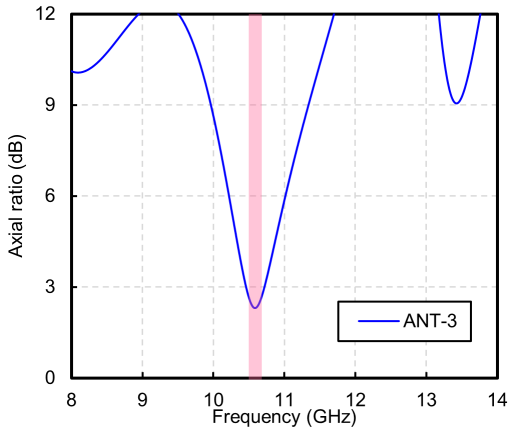

FIGURE 7. The ANT-3 axial ratio simulation.

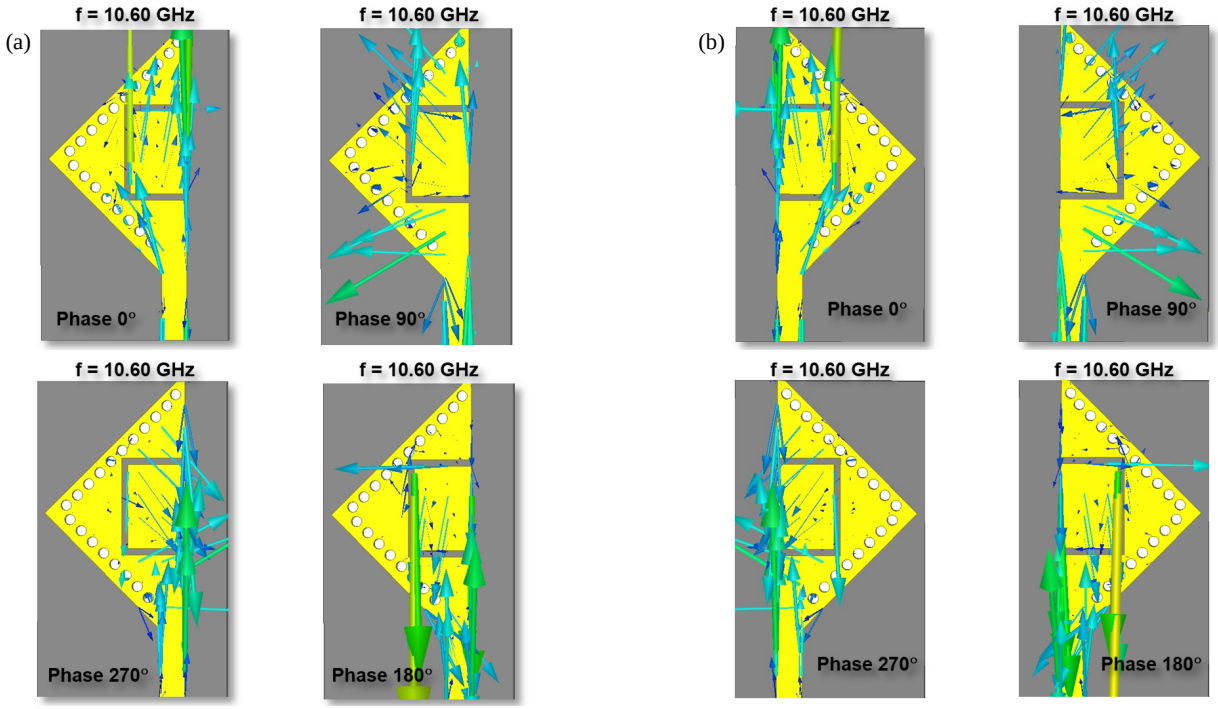

FIGURE 8. The Jsurf simulation on (a) RHCP, and (b) LHCP.

TE_{101} mode is dominant rather than the TE_{102} mode. It can be seen by the same phase spreading in Figures 4(b) and 4(d).

The electric field spreading in the second resonant occurs at 11.18 GHz as shown in Figure 5. It shows the electric field spreading combination between the strong TE_{102} mode and weak TE_{101} mode. It can be analyzed from the differentiation in electric field spreading between the upper and lower slot positions in Figures 5(a)–(d).

The third resonant electric field spreading at 12.77 GHz is depicted in Figure 6. It displays the combination of the electric field spreading between the weak TE_{102} mode and strong TE_{202} mode. The investigation shows the differentiation of the electric field spreading between the upper and lower slot segments for every 90° steps. Figure 6 is almost the same as Figure 5.

2.3. Dual Polarization

The proposed antenna design (ANT-3) features dual polarizations, including both linear and circular polarizations, as illustrated in Figure 7. The proposed antenna exhibits circular polarization, specifically right-handed circular polarization (RHCP) or left-handed circular polarization (LHCP), within the 10.46–10.72 GHz range (260 MHz), with an axial ratio of 2.46%. The RHCP antenna design is achieved by mirroring the dimensions of the LHCP antenna. The RHCP and LHCP can be analyzed based on vector surface current density Jsurf simulation on step 90° as shown in Figure 8. The Jsurf simulation has 1400 A/m maximum. By observing the changes in the surface current density vector at each phase shift of 0, 90, 180, and 270 degrees, it can be concluded that the RHCP antenna has a surface current

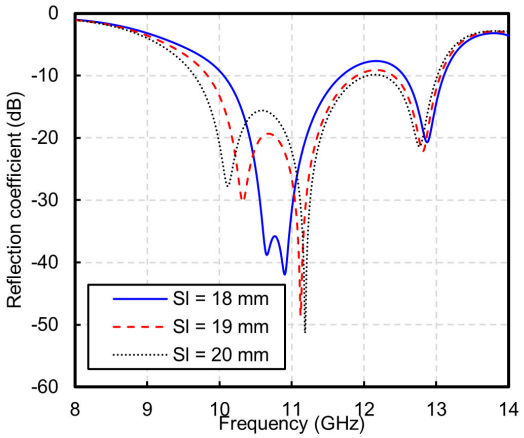

FIGURE 9. The parametric investigations for the slot length variations.

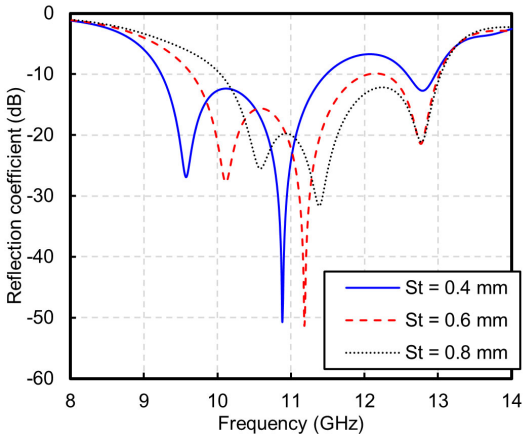

FIGURE 10. The parametric investigations for the slot thickness variations.

density vector that rotates counterclockwise. Similarly, for the LHCP antenna, the surface current density vector rotates clockwise.

2.4. Parametric Investigations

The impedance bandwidth enhancement is influenced by the slot length (S_l), slot thickness (S_t), and slot position (S_p) as shown in Figures 9–11.

The slot length is equal to one guided wavelength at a frequency of 10 GHz (20 mm). As shown in Figure 9, the impedance bandwidth becomes narrower if the slot length is less than 20 mm. The 19 mm slot length has 19.05% (9.83–11.90 GHz) of fractional bandwidth and 15.09% (10.05–11.69 GHz) for the 18 mm slot length. It is caused by the first and second resonance frequencies moving closer together, while the third resonance frequency shifts to a higher frequency. A broadband bandwidth with triple resonance frequencies disappears and becomes a dual-band impedance bandwidth.

Figure 10 shows the parametric investigations for the slot thickness. As the slot becomes thicker, the first and second resonances shift to higher frequencies while the third resonant tends to be stable. Additionally, the impedance bandwidth is broadened as the third resonance merges with the others. The best slot thickness for this proposed antenna occurs on the 0.6 mm slot thickness with 29.53% (9.67–13.02 GHz) of fractional bandwidth. The 0.4 and 0.8 mm slot thicknesses caused low fractional bandwidths of 21.62% (9.24–11.48 GHz) and 26% (10.04–13.04 GHz).

The impedance bandwidth increases as the slot moves upward. The reflection coefficient also decreases, as shown in Figure 11. The fractional bandwidth obtained is 19.89% (9.78–11.94 GHz) at the position of 6.8 mm, 29.53% (9.67–13.02 GHz) at 7.0 mm and 21.52% (9.58–11.89 GHz) at 7.2 mm. Therefore, the optimal slot position for the proposed antenna design is at 7.0 mm.

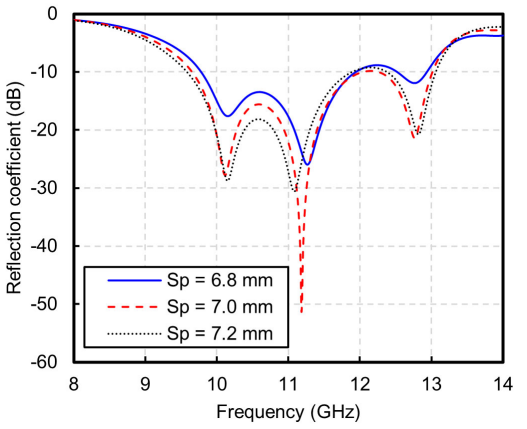

FIGURE 11. The parametric investigations for the slot position variations.

3. MEASURED AND DISCUSSION

3.1. Antenna Manufacture

The proposed antenna design is fabricated using photo etching on a Rogers Duroid RO 5880 substrate with a thickness of 1.575 mm. Rogers Duroid 5880 with 1.575 mm thickness is chosen because the thickness is not too thin. The fabrication process for the antenna (ANT-3) is illustrated in Figure 12. Figure 12 shows the top and ground layers for the RHCP antenna (Figure 12(a)), while Figure 12(b) presents the LHCP version. RHCP and LHCP are achieved by mirroring the schematic images of one another. The half-rectangular ring slot is etched on the top layer, and the ground layer is entirely covered with full copper.

3.2. Measurement

The proposed antenna design was measured using a Vector Network Analyzer (VNA) to measure the impedance bandwidth as shown in Figure 13(a). The measured fractional bandwidth of 32.05% (9.51–13.14 GHz) was achieved for the RHCP antenna design as shown in Figure 13(a). The same condition also occurs in the LHCP antenna design. The measured impedance bandwidth of 3.39 GHz (9.46–12.85 GHz) was achieved for the LHCP antenna design (ANT-3), while the simulated impedance

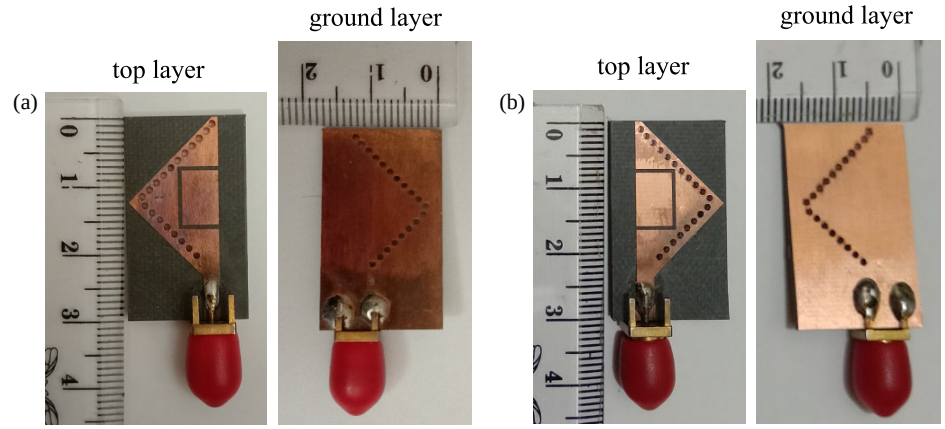

FIGURE 12. Antenna manufacture for: (a) RHCP and (b) LHCP.

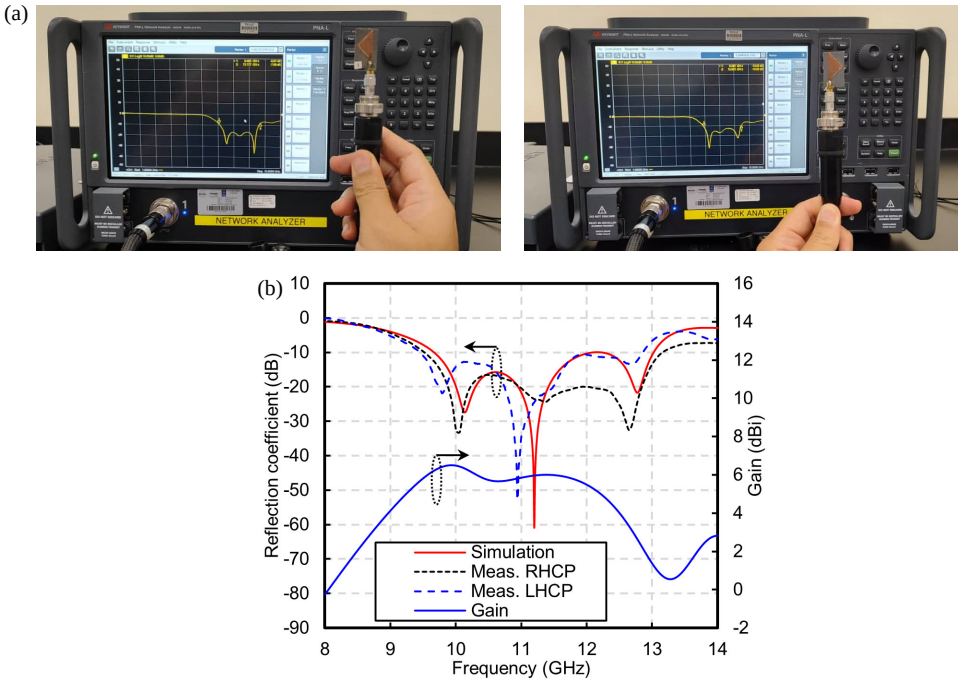

FIGURE 13. (a) The ANT-3 reflection coefficient comparison between simulation and measurement for RHCP and LHCP, and (b) reflection coefficient measurement processing.

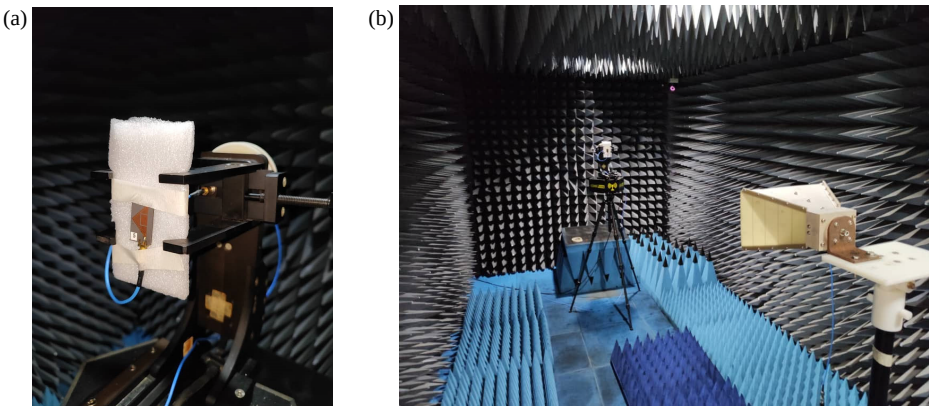

FIGURE 14. (a) The ANT-3 position for radiation pattern measurement, and (b) radiation pattern measurement in the anechoic chamber room.

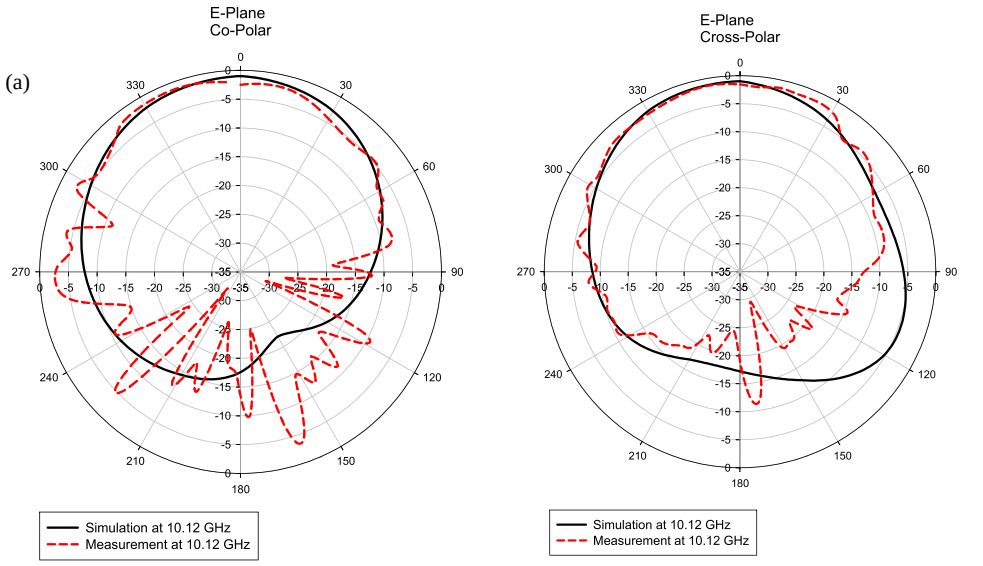
(a)
E-Plane
Co-Polar
E-Plane
Cross-Polar
Simulation at 10.12 GHz
Measurement at 10.12 GHz
Simulation at 10.12 GHz
Measurement at 10.12 GHz

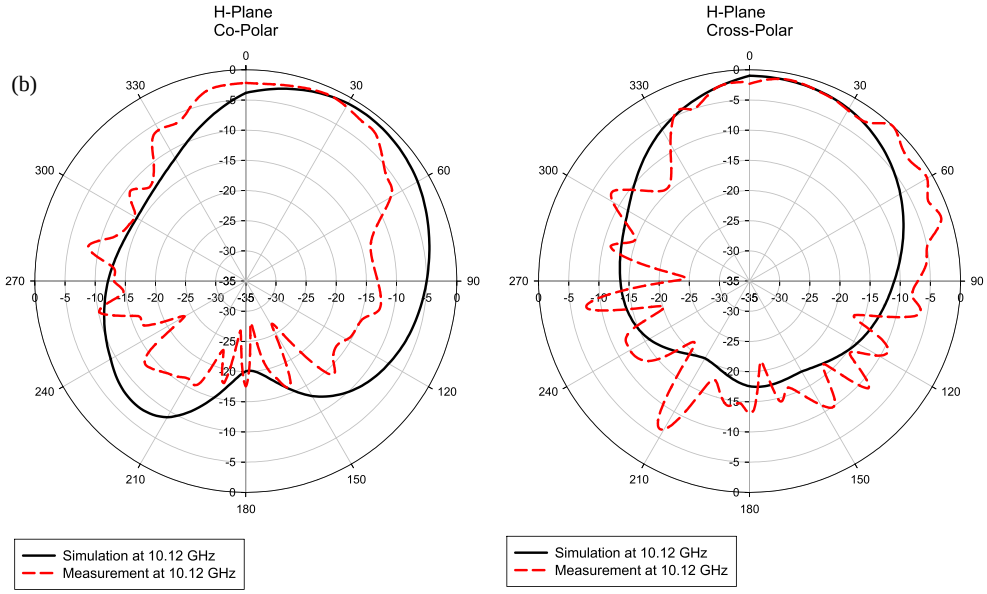
(b)
H-Plane
Co-Polar
H-Plane
Cross-Polar
Simulation at 10.12 GHz
Measurement at 10.12 GHz
Simulation at 10.12 GHz
Measurement at 10.12 GHz

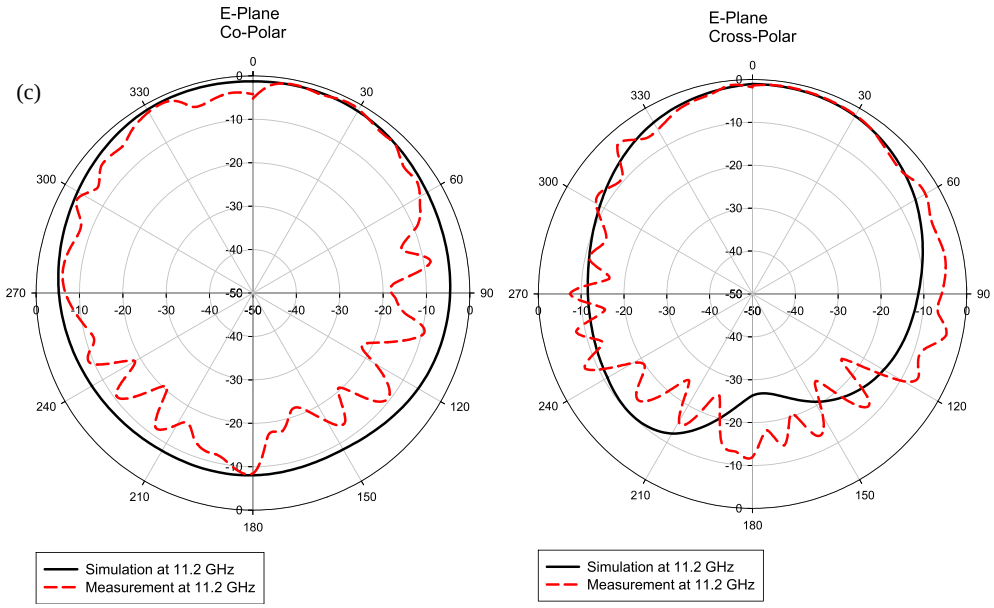
(c)
E-Plane
Co-Polar
E-Plane
Cross-Polar
Simulation at 11.2 GHz
Measurement at 11.2 GHz
Simulation at 11.2 GHz
Measurement at 11.2 GHz

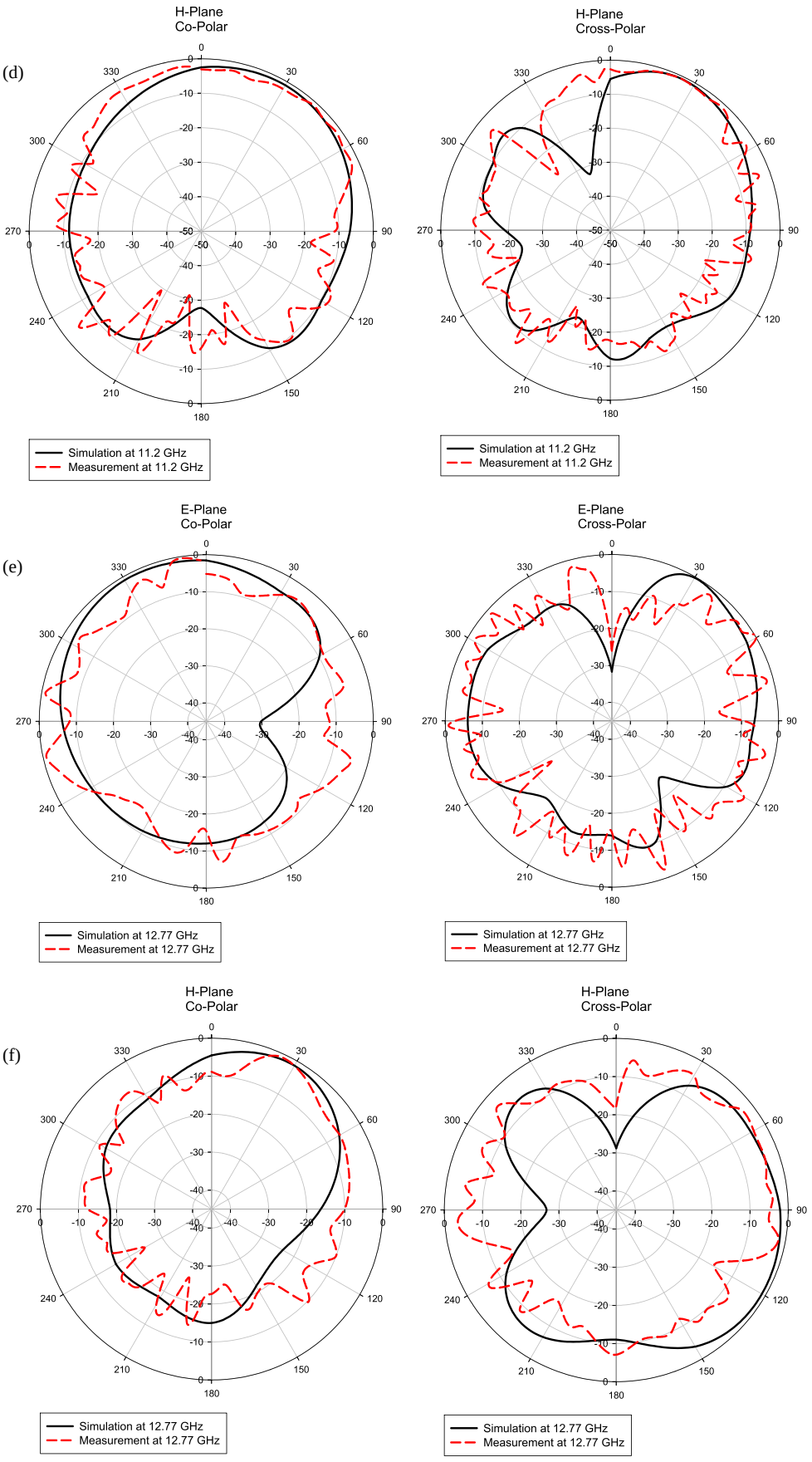

FIGURE 15. The radiation pattern simulation on: (a) 10.12 GHz for E-plane, (b) 10.12 GHz for H-plane, (c) 11.2 GHz for E-plane, (d) 11.2 GHz for H-plane, (e) 12.77 GHz for E-plane, and (f) 12.77 GHz for H-plane.

TABLE 2. A comparison of the results from the proposed antenna with previous studies related to the bandwidth enhancement method.

Reference	Slot type	Resonant	Substrate thickness (mm)	Substrate dimension (λ_0^3)	BW (GHz)	Fc (GHz)	FBW (%)
[5]	modified I-shaped	Dual	1.575	$0.94 \times 0.75 \times 0.05$	2.00	10.5	19.04
[6]	hexagonal and rectangular slots	Dual	1.60	$0.80 \times 0.57 \times 0.05$	2.18	9.79	22.27
[32]	epsilon shaped slot	Triple	1.575	$0.81 \times 0.56 \times 0.03$	0.73	5.45	13.29
[35]	A half-circular slot	Dual	0.508	$0.61 \times 0.24 \times 0.04$	3.53	27.5	1.84
[36]	A half-pentagon slot	Quad	1.575	$1.37 \times 0.56 \times 0.05$	3.46	10.87	31.83
[37]	Triangular slot	Dual	1.575	$0.38 \times 0.38 \times 0.02$	0.38	3.85	9.87
[38]	Rectangular and C-slot	Dual	1.575	$0.67 \times 0.34 \times 0.03$	0.88	6.15	14.31
This Work	**A half-rectangular ring slot**	**Triple**	**1.575**	$\mathbf{0.95 \times 0.57 \times 0.05}$	**3.63**	**11.33**	**32.05**

Note: λ_0 = The wavelength in the free-to-air for the lowest frequency

bandwidth of the LHCP antenna design was 3.35 GHz (9.67–13.02 GHz). The reflection coefficient comparison between simulation and measurement is shown in Figure 13(b). The measured impedance bandwidth is wider than the simulated one. However, the consistency of the triple resonance frequency was achieved in both simulation and measurement, although there was a slight shift. The shift was caused by the difference in conditions between simulation and measurement. The simulation has a very ideal condition compared to the fabrication condition. The proposed antenna has a 6.5 dBi gain simulation on 9.93 GHz with linear polarization.

Figure 14(a) shows the ANT-3 position for radiation pattern measurement in the anechoic chamber room while Figure 14(b) shows radiation pattern measurement processing. We used a linear horn antenna because the ARBW simulation of the proposed antenna was small. The linear horn antenna is available enough for measurement processing. Simulation and measurement comparison of radiation patterns is displayed in Figure 15 for E-plane and H-plane on 10.12 GHz, 11.2 GHz, and 12.77 GHz. The E-plane has a higher gain than the H-plane. The comparison of radiation patterns between simulation and measurement shows a similar resemblance even for the E-plane and H-plane. A slight shift occurs due to a change in the radiation pattern during measurement. However, this is not very significant. A minor shift in the back lobe of the radiation pattern is caused by reflections from the antenna holder. The slight inconsistency in the radiation shape is due to the measurement unit's sensitivity and susceptibility at higher frequencies. However, simulated and measured radiation patterns exhibit a similar shape and beam angle.

Table 2 presents a comparison between the results of the proposed broadband HMSIW antenna and previous studies that focused on bandwidth enhancement. While the proposed broadband HMSIW antenna uses the same substrate thickness (1.575 mm) as in other research, it achieves a broader bandwidth than the others. The fractional bandwidth of the proposed antenna is almost the same as the previous research [34]. However, the proposed antenna design offers a single inner cavity with a simple half-rectangular ring slot shape. It makes an easy analysis of TE mode in the single cavity.

4. CONCLUSION

A simple, low-profile, compact, and broadband antenna has been presented in this paper. The antenna design utilizes a single-cavity HMSIW structure and achieves a broadband impedance bandwidth with over 30% fractional bandwidth in the X-band frequency range. The broadband performance results from the merging of triple resonances, induced by a half-rectangular ring slot on the top layer of the cavity for radiation. The half-rectangular ring slot is optimized in terms of slot length, thickness, and position. The triple resonances are achieved through a combination of neighboring TE modes. The strong and weak resonance combinations can be analyzed by examining the electric field spreading differences across the segments of the half-rectangular ring slot. The proposed antenna has a small dimension with a higher fractional bandwidth than other existing antennas in the literature. Good agreement is observed between the simulation and measurement results. The measured fractional bandwidth is 32.05% (9.51–13.14 GHz) with a uniform radiation pattern and low-profile planar antenna. The proposed antenna design is a suitable option for multi-band applications in the X-band.

ACKNOWLEDGEMENT

This research was supported/partially supported by Universitas Mercu Buana, Kerjasama Luar Negeri number 02-5/702/B-SPK/V/2024.

REFERENCES

[1] Aparna, E., G. Ram, and G. A. Kumar, "Review on substrate integrated waveguide cavity backed slot antennas," *IEEE Access*, Vol. 10, 133 504–133 525, 2022.

[2] Yun, S., D.-Y. Kim, and S. Nam, "Bandwidth and efficiency enhancement of cavity-backed slot antenna using a substrate removal," *IEEE Antennas and Wireless Propagation Letters*, Vol. 11, 1458–1461, 2012.

[3] Yong, W. Y., A. Haddadi, T. Emanuelsson, and A. A. Glazunov, "A bandwidth-enhanced cavity-backed slot array antenna for mmWave fixed-beam applications," *IEEE Antennas and Wireless Propagation Letters*, Vol. 19, No. 11, 1924–1928, 2020.

[4] Cheng, T., W. Jiang, S. Gong, and Y. Yu, "Broadband SIW cavity-backed modified dumbbell-shaped slot antenna," *IEEE Antennas and Wireless Propagation Letters*, Vol. 18, No. 5, 936–940, 2019.

[5] Srinivas, L., G. A. Kumar, and G. Ram, "A novel design of modified I-shaped low profile broadband cavity-backed SIW slot antenna," *Journal of Electromagnetic Waves and Applications*, Vol. 38, No. 6, 724–737, 2024.

[6] Vinodha, E., "A broadband low profile SIW cavity-backed antenna loaded with hexagonal and rectangular slots for 'X' band application," *Analog Integrated Circuits and Signal Processing*, Vol. 118, No. 2, 307–315, 2024.

[7] Sepryanto, S., S. Attamimi, and F. Sirait, "Perancangan antenna mikrostrip SIW cavity-backed modified dumbell-shaped slot untuk pengaplikasian pada 5G," *J. Teknol. Elektro.*, Vol. 11, No. 2, 115–119, 2020.

[8] Patil, S. M. and R. Venkatesan, "Bandwidth enhancement of substrate integrated waveguide cavity-backed half bow-tie complementary-ring slot antenna for Ku-band applications," *Alexandria Engineering Journal*, Vol. 81, 46–54, 2023.

[9] Chaturvedi, D., A. A. Althuwayb, and A. Kumar, "Bandwidth enhancement of a planar SIW cavity-backed slot antenna using slot and metallic-shorting via," *Applied Physics A*, Vol. 128, No. 3, 193, 2022.

[10] Murad, N. A., M. W. Almeshehe, O. Ayop, and M. K. A. Rahim, "Wideband metamaterial substrate integrated waveguide antenna for millimeterwave applications," in *2020 IEEE International RF and Microwave Conference (RFM)*, 1–4, Kuala Lumpur, Malaysia, 2020.

[11] Bordbar, A., F. Mohajeri, and Z. Ghorbani, "Gain and bandwidth enhancement of a metamaterial loaded antipodal Vivaldi antenna fed by substrate integrated waveguide," *Radioengineering*, Vol. 31, No. 2, 193–200, 2022.

[12] Banerjee, S. and S. K. Parui, "Bandwidth improvement of substrate integrated waveguide cavity-backed slot antenna with dielectric resonators," *Microsystem Technologies*, Vol. 26, No. 4, 1359–1368, 2020.

[13] Zhao, R., B. Liu, Y. Ma, W. Xing, and X. Sun, "Design of a substrate-integrated waveguide based slot-pair array antenna for bandwidth enhancement," *IET Microwaves, Antennas & Propagation*, Vol. 14, No. 13, 1481–1487, 2020.

[14] Gorai, A., A. Deb, J. R. Panda, and R. Ghatak, "Millimeter wave/5G multiband SIW antenna with metasurface loading for circular polarization and bandwidth enhancement," *Journal of Infrared, Millimeter, and Terahertz Waves*, Vol. 43, No. 5, 366–383, 2022.

[15] Astuti, D. W. and E. T. Rahardjo, "Size reduction of cavity backed slot antenna using half mode substrate integrated waveguide structure," in *2018 4th International Conference on Nano Electronics Research and Education (ICNERE)*, 1–4, Hamamatsu, Japan, 2018.

[16] Banerjee, S., S. D. Mazumdar, S. Chatterjee, and S. K. Parui, "Half mode semi-hexagonal SIW antennas and arrays for cellular V2X communication," *Microsystem Technologies*, Vol. 27, No. 10, 3639–3651, 2021.

[17] Pramodini, B. and D. Chaturvedi, "Miniaturized inverted L-shaped slot antenna using HMSIW technology," in *2023 2nd International Conference on Paradigm Shifts in Communications Embedded Systems, Machine Learning and Signal Processing (PCEMS)*, 1–4, Nagpur, India, 2023.

[18] Niu, B.-J. and J.-H. Tan, "Compact self-isolated MIMO antenna system based on quarter-mode SIW cavity," *Electronics Letters*, Vol. 55, No. 10, 574–576, 2019.

[19] Sun, Y.-X., D. Wu, X. S. Fang, and N. Yang, "Compact quarter-mode substrate-integrated waveguide dual-frequency millimeter-wave antenna array for 5G applications," *IEEE Antennas and Wireless Propagation Letters*, Vol. 19, No. 8, 1405–1409, 2020.

[20] JayaPrakash, V. and D. S. Chandu, "Compact four-element quarter mode circular SIW based MIMO antenna with enhanced isolation," *Wireless Personal Communications*, Vol. 133, No. 1, 625–640, 2023.

[21] Casula, G. A., G. Montisci, and G. Muntoni, "A novel design for dual-band wearable textile eighth-mode SIW antennas," *IEEE Access*, Vol. 11, 11 555–11 569, Feb. 2023.

[22] Shi, H., Y. Wang, S. Zhang, H. Wang, and H. Tang, "Compact eighth-mode substrate integrated waveguide filtering antenna with cross C-slots," in *2023 International Conference on Microwave and Millimeter Wave Technology (ICMMT)*, 1–3, Qingdao, China, 2023.

[23] Iqbal, A., M. Al-Hasan, I. B. Mabrouk, and T. A. Denidni, "Highly miniaturized eighth-mode substrate-integrated waveguide self-quadruplexing antenna," *IEEE Antennas and Wireless Propagation Letters*, Vol. 22, No. 9, 2275–2279, 2023.

[24] Rani, A. and S. Das, "A high-isolation SIW self-octaplexing antenna with independent frequency tuning capability," *IEEE Antennas and Wireless Propagation Letters*, Vol. 23, No. 6, 1954–1958, 2024.

[25] Kumari, P. and S. Das, "A wideband circularly polarized SIW MIMO antenna based on coupled QMSIW and EMSIW resonators for sub-6 GHz 5G applications," *IEEE Antennas and Wireless Propagation Letters*, Vol. 23, No. 10, 2979–2983, 2024.

[26] Sujatha, M. N., K. S. Lekhanashree, S. Gnanavi, S. B. Naik, and D. Raj, "Design and analysis of self triplexing antenna using quarter mode and eighth mode substrate integrated waveguide cavities," in *2024 International Conference on Smart Systems for applications in Electrical Sciences (ICSSES)*, 1–4, Tumakuru, India, 2024.

[27] Kumari, P. and S. Das, "A MIMO antenna system using self-decoupled EMSIW dual-beam antenna elements," *IEEE Access*, Vol. 10, 1339–1345, 2021.

[28] Ali, S. A., M. Wajid, M. Hashmi, and M. S. Alam, "A compact size and high isolation dual-band MIMO antenna using EMSIW," in *2022 5th International Conference on Multimedia, Signal Processing and Communication Technologies (IMPACT)*, 1–5, Aligarh, India, 2022.

[29] Thapa, S. K., C. Baichuan, A. Barakat, and R. K. Pokharel, "Experimental study on the effect of feeding topology of 60 GHz sixteenth mode SIW cavity resonator in CMOS technology," in *2022 Asia-Pacific Microwave Conference (APMC)*, 384–386, Yokohama, Japan, Nov. 2022.

[30] Thapa, S. K., R. K. Pokharel, B. Chen, T. Fukuda, and A. Barakat, "Millimeter-wave high Q-factor sixteenth mode SIW cavity resonator implemented in 0.18-µm CMOS technology," in *2022 IEEE/MTT-S International Microwave Symposium — IMS 2022*, 560–563, Denver, CO, USA, Jun. 2022.

[31] Choudhury, S. and A. Mohan, "Electrically small 64th-mode substrate-integrated waveguide monopole antenna," *Electronics Letters*, Vol. 52, No. 8, 580–581, 2016.

[32] Chaturvedi, D., A. Kumar, and S. Raghavan, "Wideband HMSIW-based slotted antenna for wireless fidelity application," *IET Microwaves, Antennas & Propagation*, Vol. 13, No. 2, 258–262, 2019.

[33] Kumar, L., V. Nath, and B. V. R. Reddy, "An HMSIW cavity-backed wide-band antenna for 5G mm-Wave band," in *2023 World Conference on Communication & Computing (WCONF)*,

1–6, Raipur, India, 2023.

[34] Astuti, D. W., M. Muslim, U. Umaisaroh, H. A. Majid, and S. Alam, "Broadband HMSIW antenna using a demi hexagonal ring slot for X-band application," *Sinergi (Indonesia)*, Vol. 29, No. 1, 73–82, 2025.

[35] Wu, Q., H. Wang, C. Yu, and W. Hong, "Low-profile circularly polarized cavity-backed antennas using SIW techniques," *IEEE Transactions on Antennas and Propagation*, Vol. 64, No. 7, 2832–2839, 2016.

[36] Astuti, D. W., Y. Wahyu, F. Y. Zulkifli, and E. T. Rahardjo, "Hybrid HMSIW cavities antenna with a half-pentagon ring slot for bandwidth enhancement," *IEEE Access*, Vol. 11, 18 417–18 426, Feb. 2023.

[37] Astuti, D. W., M. Asvial, F. Y. Zulkifli, and E. T. Rahardjo, "Bandwidth enhancement on half-mode substrate integrated waveguide antenna using cavity-backed triangular slot," *International Journal of Antennas and Propagation*, Vol. 2020, No. 1, 1212894, 2020.

[38] Astuti, D. W., I. Simanjuntak, T. Firmansyah, D. A. Cahyasiwi, Y. Natali, *et al.*, "Bandwidth enhancement for half mode substrate integrated waveguide antenna using defected ground structures," *International Journal of Electronics and Telecommunications*, Vol. 69, No. 3, 449–454, 2023.

[39] Dashti, H. and M. H. Neshati, "Development of low-profile patch and semi-circular SIW cavity hybrid antennas," *IEEE Transactions on Antennas and Propagation*, Vol. 62, No. 9, 4481–4488, 2014.

[40] Agneessens, S., "Coupled eighth-mode substrate integrated waveguide antenna: Small and wideband with high-body antenna isolation," *IEEE Access*, Vol. 6, 1595–1602, 2017.

[41] Zhou, J. and M. Yang, "A low-profile eighth-mode SIW antenna with dual-sense circular polarization, enhanced bandwidth and simple structure," *IEEE Access*, Vol. 9, 144 375–144 384, 2021.

[42] Niu, B.-J. and J.-H. Tan, "Bandwidth enhancement of low-profile SIW cavity antenna using fraction modes," *Electronics Letters*, Vol. 55, No. 5, 233–234, 2019.

[43] Xu, F. and K. Wu, "Guided-wave and leakage characteristics of substrate integrated waveguide," *IEEE Transactions on Microwave Theory and Techniques*, Vol. 53, No. 1, 66–73, 2005.

[44] Pozar, D. M., *Microwave Engineering*, 4th ed., John Wiley & Sons, 2012.